Electric field gradients at ^{111}Cd in binary oxides

1993 J. Phys.: Condens. Matter 5 4111

(http://iopscience.iop.org/0953-8984/5/25/002)

J. Phys.: Condens. Matter 5 (1993) 4111–4124. Printed in the UK

Electric field gradients at ^{111}Cd in binary oxides

D Wiarda, M Uhrmacher, A Bartos and K P Lieb

II.Physikalisches Institut, Universität Göttingen, D-3400 Göttingen, Federal Republic of Germany

Received 15 September 1992, in final form 19 March 1993

Abstract. The electric field gradients (EFGs) of ^{111}Cd at substitutional sites in binary oxides of different crystal structures obtained in perturbed angular correlation (PAC) experiments are collected and compared to point charge model (PCM) calculations. The error of the calculated EFGs is estimated from the experimental error in the crystal parameters. The PCM seems to be a good approximation for oxides with bond lengths exceeding $d \simeq 2.1$ Å and here the theoretical shielding factor γ_∞ can be used. The application of radially dependent shielding factors for $d \leqslant 2.1$ Å where covalent bonding prevails is discussed.

1. Introduction

In recent years a large number of electric field gradients (EFGs) of ^{111}Cd impurity atoms on substitutional cation sites in binary oxides has been collected [1]. In most cases the ^{111}In mother activity was implanted into polycrystalline samples and appropriate annealing procedures ensured the ^{111}In probe to be at undisturbed substitutional sites. All next neighbours of the impurity probe will be oxygen ions, their number, distance and spatial distribution being determined by the actual oxide matrix. Furthermore, many of the oxides studied show predominantly ionic bonding. Therefore the large sample of PAC data collected for ^{111}In/^{111}Cd in oxides may serve as a basis for empirical comparisons between the hyperfine interaction (HFI) parameters found with different oxygen coordinations. As ^{111}In/^{111}Cd is an impurity atom, one might ask whether it acts as an 'ideal observer' or to what extent it disturbs its local environment. Therefore it is important to investigate the influence of the probe atom itself on the measured EFG as well as on the local oxygen configuration. Several oxides exhibiting magnetic phase transitions have been shown to display a critical behaviour independent of the chosen probe atom [2].

The clearest dependence of the EFG on the lattice constant was found for the oxides crystallizing in the bixbyite structure [3]. This class is now well examined by PAC experiments using the ^{111}In/^{111}Cd probe [3,4]. Since In itself crystallizes as In_2O_3 in this structure (where the ^{111}In probe is *no* impurity atom), it is very promising to observe that in all other oxides of this class the PAC data correspond to *different* EFGs, and not to that of In_2O_3. Similar observations were made in other crystal classes and clearly suggest that, in fact, the impurity probe ^{111}In/^{111}Cd behaves as an observer.

The exact calculation of the EFG in a crystal can be extracted, in principle, from self-consistent field calculations of the total wave function. This has been done in metals with nearly all approximations of wave functions and potentials (see for example [5]). In oxides these calculations are much more difficult as the crystal structure is normally more complicated [6]. Detailed theoretical work has been carried out concerning the EFG of Al in

0953-8984/93/254111+14$07.50

Al_2O_3 (see [7] and references therein). Blaha *et al* [8, 9] used the LAPW method to calculate the EFG in different oxides, but not for impurity atoms. At present, Kranefeld and Fritsche [10] are expanding this method in order to calculate the EFG of ^{111}Cd in TiO_2. Nagel [11] used an MSX_α-cluster method for calculating the EFG of ^{111}Cd impurity atoms in Cu_2O and Ag_2O. In the case of α-Fe_2O_3, the EFG of Fe has been calculated by Beri *et al* [12]. To our knowledge, no self-consistent field calculations of the EFG at ^{111}Cd sites have been performed so far for the oxides discussed in this paper, with the exceptions given above.

Alternatively, in the case of a pure ionic compound the point charge model (PCM) may work. In fact, it is often the only access to theoretical predictions. It is the aim of this paper to compile the experimental PAC data on oxides and to compare them with PCM calculations. This will to some extent answer the following questions: Under what conditions can the 'simple' PCM be used? What are its limitations and for what reasons? What other effects have to be taken into account? As an example, we mention the cases of β-Fe_2O_3 and Mn_2O_3: both oxides have the *same* lattice structure and lattice constant, but show quite different experimental EFGs [4], due to their different covalencies. At close distances to the next neighbours, covalent bonding is expected and the spatial distribution of the electrons should influence the EFG. The electronic shell of the probe atom itself also has a strong influence on the EFG. This can be taken into account by *ab initio* EFG calculations which have recently become feasible in the case of oxides [7, 13, 8] The PCM may incorporate these effects by the use of proper shielding factors [14–16].

2. The electric field gradient

In this paper we are concerned with the EFG measured via its interaction with the electric quadrupole moment Q of the intermediate level of the probe nucleus ^{111}Cd. The EFG is the second derivative of the electric potential φ and is therefore a symmetric tensor of rank two:

$$V'_{ij} = \partial^2\varphi/\partial x_i \partial x_j \tag{1}$$

and the trace obeys the inhomogeneous Poisson equation

$$V'_{11} + V'_{22} + V'_{33} = 4\pi\rho \tag{2}$$

where ρ is the charge distribution of the probe nucleus. This tensor can be divided into two symmetric tensors [5]

$$V_{ij} = V'_{ij} - \delta_{ij}\Delta\varphi \tag{3}$$

where V_{ij} is a traceless tensor.

An external field leads to a splitting of the m substates of the intermediate $5/2^+$ state in ^{111}Cd, giving rise to a time dependent modulation of the measured γ intensities, as described in [17, 18]. An external charge distribution overlapping with the charge distribution ρ of the probe nucleus will not cause any changes in the relative distances of the m substates [5]. Thus, in the case of PAC measurements it is sufficient to discuss the traceless symmetric tensor V_{ij}. This tensor can be diagonalized and two numbers are sufficient to define it. Ordering the eigenvalues as

$$|V_{11}| \leqslant |V_{22}| \leqslant |V_{33}| \tag{4}$$

the coupling constant

$$\nu_Q = eQV_{33}/h \tag{5}$$

as a measure of the highest eigenvalue V_{33}, and the asymmetry parameter

$$\eta = (V_{11} - V_{22})/V_{33} \tag{6}$$

are normally used to define the V_{ij}.

3. The EFG data base in different crystalline structures

Nearly all PAC data with ^{111}In/^{111}Cd in oxides have been obtained by $^{111}In^+$ implantations into polycrystalline samples at energies around 400 keV. The phases were usually confirmed via x-ray diffraction analysis. As the probe atom normally forms positive ions, it will substitute cations in the oxides discussed. In the following, only HFI parameters of probe atoms on substitutional sites are discussed. For an inspection of these assignments, the reader should refer to the literature given in the tables. Effects connected to the electron-capture decay of $^{111}In \rightarrow {}^{111}Cd$, so-called 'after effects' are not considered in this paper. If the measuring temperature is chosen sufficiently high, the hyperfine parameters ν_Q and η will not be affected by additional dynamic interactions, i.e. all PAC data were consistently analysed via *static* HFI.

3.1. Bixbyite structure

The oxides crystallizing in the bixbyite structure can be described in the space group $Ia3$ where two inequivalent cation sites exist: 25% of the cations are surrounded by a nearly regular oxygen octahedron (D site) and 75% by an irregular sixfold oxygen coordination (C site). In the PAC spectra taken in this class of oxides two main fractions are visible, attributed to the two inequivalent cation sites, one with an asymmetry parameter $\eta \simeq 0$ (D site) and one with $\eta \simeq 0.7$ (C site). The experimental hyperfine parameters are given in table 1, along with the references.

3.2. Corundum structure

In the oxides crystallizing in the corundum structure each cation is surrounded by a nearly regular oxygen octahedron. The bond lengths between cations and oxygen ions are rather small (1.91–2.02 Å) as compared to the oxides crystallizing in the bixbyite structure. The corundum structure is interesting as several theoretical papers are devoted to calculating the EFG in Al_2O_3 [7, 19–25]. In nearly all PAC spectra one fraction with $\eta \simeq 0$ and a coupling constant of $\nu_Q = 130$–200 MHz was found. For the measured HFI parameters of Ti_2O_3 no unambiguous assignment to the lattice sites could be made until now, so here two values are given in table 1.

3.3. Rutile structure

The rutile structure is one of the most common crystal structures for AB_2 compounds with octahedral coordination [26]. The symmetry is tetragonal with a flat unit cell containing two formula units. In the regular rutile structure the cations are surrounded by six oxygen ions, except in the case of the low-temperature form of NbO_2, which crystallizes in a distorted rutile structure. Here two inequivalent cation sites exist. Accordingly, a single EFG is found in the oxides TiO_2, VO_2 and SnO_2 with $\eta \simeq 0.18$ and two EFGs in the case of NbO_2. The experimental values and the references are given in table 1.

Table 1. For several oxides with different crystal structures the table first shows the average distance of a cation to the next-neighbour oxygen ions. The experimental HFI parameters from PAC experiments are given which have been attributed to a substitutional probe location. The next columns display the results of the PCM calculations including the error due to the uncertainty of the crystal parameters. Using the standard shielding factor β_∞ the PCM prediction can be calculated. The last two columns give the ratios which are used in figures 4 and 5.

Sample			Experiment			PCM calculation				
Oxide	$\langle d \rangle$ (Å)	Reference	ν_Q(exp) (MHz)	η(exp)	Reference	ν_Q(latt) (MHz)	η(pcm)	ν_Q(pcm) = $\beta_\infty \nu_Q$(latt)	$\frac{\nu_Q(\text{exp})}{\nu_Q(\text{latt})}$	$\frac{\eta(\text{exp})}{\eta(\text{pcm})}$
Bixbyite, C site										
In_2O_3	2.17	[33][a]	118(1)	0.71(2)	[3]	3.27(36)	0.80(18)	99(11)	36(4)	0.89(45)
	2.19	[33][b]	118(1)	0.71(2)	[3]	2.93(36)	0.65(18)	89(11)	40(5)	1.09(61)
Y_2O_3	2.28	[39]	89(2)	0.77(2)	[3]	2.34(6)	0.64(6)	71(2)	38(2)	1.20(42)
Sc_2O_3	2.12	[37]	132(1)	0.71(1)	[3]	2.13(18)	0.30(18)	65(5)	62(6)	2.4(18)
	2.12	[38]	132(1)	0.71(1)	[3]	2.54(3)	0.95(3)	77(1)	52(1)	0.75(3)
Dy_2O_3	2.29	[40]	82(2)	0.81(5)	[3]	3.31(63)	0.59(27)	100(19)	25(5)	1.37(71)
Yb_2O_3	2.24	[41]	97(1)	0.75(2)	[3]	2.44(9)	0.71(9)	75(3)	40(2)	1.06(16)
	2.25	[42]	97(1)	0.75(2)	[3]	2.54(27)	0.77(9)	77(8)	38(5)	0.97(14)
Ho_2O_3	2.28	[41]	81(2)	0.82(3)	[43]	4.04(36)	0.82(9)	122(11)	20(2)	1.00(15)
Gd_2O_3	2.32	[44]	64(3)	0.98(4)	[43]	2.49(27)	0.71(9)	75(8)	26(4)	1.38(23)
Sm_2O_3	2.35	[44]	58(2)	0.91(2)	[43]	2.40(27)	0.71(9)	73(3)	24(4)	1.28(19)
Mn_2O_3	2.04	[45]	208(1)	0.68(1)	[4]	12.85(9)	0.27(9)	389(3)	16.2(2)	2.52(88)
β-Fe_2O_3	2.04	[45, 46]	165(1)	0.63(1)	[4]	12.85(9)	0.27(9)	389(3)	12.8(2)	2.33(81)
Bixbyite, D site										
In_2O_3	2.19	[33][a]	154(1)	0	[3]	5.00(45)	0	151(14)	31(3)	—
	2.16	[33][b]	154(1)	0	[3]	4.65(45)	0	141(14)	40(5)	—
Y_2O_3	2.28	[39]	150(2)	0	[3]	5.00(9)	0	151(3)	30(1)	—
Sc_2O_3	2.13	[37]	166(2)	0	[3]	5.11(27)	0	155(8)	33(2)	—
	2.12	[38]	166(2)	0	[3]	4.69(5)	0	142(2)	32(1)	—
Dy_2O_3	2.28	[40]	149(2)	0	[3]	7.57(89)	0	229(27)	20(3)	—
Yb_2O_3	2.25	[41]	154(2)	0	[3]	5.07(18)	0	154(5)	30(2)	—
	2.25	[42]	154(2)	0	[3]	4.44(27)	0	134(8)	35(3)	—
Ho_2O_3	2.28	[41]	149(4)	$\leqslant$0.03	[43]	6.05(45)	0	183(14)	25(3)	—
Gd_2O_3	2.34	[44]	145(5)	0	[43]	4.89(36)	0	148(11)	30(3)	—
Sm_2O_3	2.36	[44]	144(3)	0	[43]	4.73(36)	0	143(11)	30(3)	—
Mn_2O_3	2.003	[45]	116(1)	0.11(2)	[4]	1.70(9)	0	52(3)	68(4)	—
β-Fe_2O_3	2.003	[45, 46]	183(1)	0.05(2)	[4]	1.70(9)	0	52(3)	108(6)	—
Rutile										
TiO_2	1.958	[26]	105(1)	0.18(1)	[47]	1.15(22)	0.48(31)	35(7)	91(18)	0.38(26)
SnO_2	2.053	[26]	117(1)	0.18(2)	[48]	3.43(2)	0.18(10)	104(1)	34(1)	1.00(66)
VO_2	1.919	[49]	89(1)	0.20(2)	[50]	12(8)	0.68(17)	363(242)	7(5)	0.29(10)
NbO_2	1.93	[51, 52]	201(19)	0.30(4)	[53, 54]	9(3)	0.55(35)	272(91)	22(10)	0.55(42)
			179(15)	0.50(14)		10(4)	0.35(35)	303(121)	18(9)	1.4(18)
Corundum										
Al_2O_3	1.91	[26]	194(3)	0.26(4)	[55]	2.49(10)	0	75(3)	78(4)	—
Cr_2O_3	1.98	[26]	149(2)	$\leqslant$0.16	[56, 57]	1.90(10)	0	58(3)	78(5)	—
Rh_2O_3	2.041	[58]	131(1)	0.19(4)	[34]	1.10(97)	0	33(29)	119(106)	—
Ti_2O_3	2.04	[26]	168(1)[c]	$\leqslant$0.05	[47]	4.93(5)	0	149(2)	34(1)	—
			137(2)[c]	0.08(5)	[47]	4.93(5)	0	149(2)	28(1)	—
V_2O_3	2.07	[26]	126(1)	0	[59]	0.78(5)	0	24(2)	161(11)	—
α-Fe_2O_3	2.02	[26]	159(3)	0	[60]	1.66(15)	0	50(5)	96(11)	—
α-Ga_2O_3	2.00	[61]	182(2)	0	[62]	3.41(31)	0	103(9)	53(6)	—

Table 1. (continued)

Sample			Experiment			PCM calculation				
Oxide	⟨d⟩ (Å)	Reference	ν_Q(exp) (MHz)	η(exp)	Reference	ν_Q(latt) (MHz)	η(pcm)	ν_Q(pcm) = $\beta_\infty \nu_Q$(latt)	ν_Q(exp) / ν_Q(latt)	η(exp) / η(pcm)
Cuprite										
Cu_2O	1.84	[26]	124(1)	0	[63]	31.5(6)	0	954(18)	3.9(1)	—
Ag_2O	2.04	[26]	129(4)	0	[27]	23.3(2)	0	705(6)	5.5(2)	—
Spinel, tetra- and octahedral sites										
Co_3O_4	1.93	[64]	0	0	[65]	0	0	0	—	—
	1.915	[64]	146(1)	⩽0.1	[65]	⩽0.8	0	⩽24	⩾183	—
Mn_3O_4	2.55	[66]	187(2)	0.89(1)	[4]	3.51(9)	0	106(3)	53(2)	—
	2.60	[66]	87(1)	0.13(6)	[4]	7.76(36)	0.07(9)	235(11)	11(1)	—
Fe_3O_4	1.93	[67]	0	0	[70]	12(18)	0	363(91)	0	—
	1.915	[67]	42(2)	0	[70]	33(1)	0	989(30)	1.3(1)	—
Tenorite										
CuO	2.23	[68]	420(1)	0.42(1)	[63]	21.3(1)	0.282(1)	645(1)	19.7(1)	1.49(9)
AgO	2.27	[26]	323(5)	0.00(5)	[27]	17.2(1)	0.46(2)	521(3)	18.8(4)	0
Sodium chloride structure										
CoO	2.13	[26]	0	0	[69]	0	0	0	—	—
NiO	2.08	[26]	0	0	[1]	0	0	0	—	—
FeO	2.16	[26]	0	0	[70]	0	0	0	—	—
MnO	2.22	[26]	0	0	[54]	0	0	0	—	—

[a] Cu Kα.
[b] Mo Kα.
[c] Still two assignments possible.

3.4. Spinel structure

In the normal spinel structure, there exist two cation coordinations connected with different ionic charge states. The 2^+ ions have fourfold coordination and the 3^+ ions have sixfold coordination. Both sites are relatively regular. In an inverse spinel, the 3^+ ions are situated at the tetrahedral site and at the octahedral site 2^+ and 3^+ ions are present. The distribution of the various charge states over the octahedral sites may cause a problem in the PCM calculations. Here we have chosen a mean positive charge of 2.5 for all octahedral sites. At the tetrahedral site of the normal spinel Co_3O_4 and of the inverse spinel Fe_3O_4, the probe atom ^{111}Cd has zero coupling constant. At the octahedral site the probe will find a non-vanishing EFG with an asymmetry parameter of $\eta = 0$. The normal spinel Mn_3O_4 shows a distortion at room temperature due to a collective Jahn–Teller effect. Here the PAC data exhibit rather large EFGs. The data and their references are summarized in table 1.

3.5. Tenorite and cuprite structure

In these structures the cations have fourfold or twofold coordinations. Those investigated most thoroughly are the copper oxides CuO (tenorite) and Cu_2O (cuprite). In CuO four oxygen atoms have quadratical coplanar bonding to the copper atoms, while the structure of AgO is more complicated as two inequivalent cation sites are present. However, only one HFI interaction was seen in the PAC spectra [27]. In the cuprites Cu_2O and Ag_2O two anions are linearly bonded to one cation.

3.6. Sodium chloride structure

In this structure the cations of the transitional element monoxides NiO, CoO, MnO and FeO are sixfold coordinated by a perfect octahedron of oxygen ions. In contrast to the corundum structure, the EFG produced by more distant ions also vanishes due to the perfect cubic symmetry of the lattice. Without a local distortion by the probe, a vanishing EFG is expected and also confirmed by the data. Therefore, this crystal class plays no further role in the PCM discussion, but the known data and references are incorporated in table 1 for the sake of completeness. Well defined EFGs may be found in these oxides, too, but they are caused by structural defects typical for the non-stoichiometry of these oxides.

4. PCM calculations

In the PCM the electric potential φ is calculated by assuming point charges q_n of the formal ionic charges of the anions and cations at the crystallographic locations. For a probe atom located at the origin one calculates

$$V_{ij}^{\mathrm{PCM}} = \sum_n q_n \frac{3x_n^i x_n^j - \delta_{ij}|x_n|^2}{|x_n|^5} \tag{7}$$

where n runs over all ions in the crystal and q_n is the formal charge of the ion. In the past, several methods have been used to calculate this lattice sum [19, 20, 23, 28] the convergence of which has to be tested. A regular lattice is described by the three lattice vectors $\boldsymbol{a}$, $\boldsymbol{b}$ and $\boldsymbol{c}$, the angles α, β and γ between the three lattice vectors and the vectors $(r_k)_{k=1}^n$ of the basis [29]. Often the basis is given by the point symmetry groups characteristic of the specific space group. Three parameters (x, y and z) describe the exact position in the unit cell of an atom having the formal charge q_k. The net charge in the unit cell is zero due to the electrical neutrality of the crystal. The positions are usually determined by x-ray or neutron diffraction. For a regular lattice the summation of equation (7) is therefore given by

$$V_{ij}^{\mathrm{PCM}} = \sum_{l_1,l_2,l_3} \sum_{k=1}^{n} q_k \frac{3r_{\mathbf{l},k}^i r_{\mathbf{l},k}^j - \delta_{ij} r_{\mathbf{l},k}^2}{r_{\mathbf{l},k}^5} \tag{8}$$

where $r_{\mathbf{l},k}$ is the length of

$$r_{\mathbf{l},k} = (l_1 + r_k^1)\boldsymbol{a} + (l_2 + r_k^2)\boldsymbol{b} + (l_3 + r_k^3)\boldsymbol{c} \tag{9}$$

and the l_m ($m = 1, 2, 3$) are integers accounting for the translation invariance of the lattice. Bersohn [19] and Sharma and Das [21] made a 'polyhedron summation' of equation (8) by summing over all ions situated in the largest sphere contained in the polyhedron

$$(l_1\boldsymbol{a} + l_2\boldsymbol{b} + l_3\boldsymbol{c})_{l_i \leqslant \pm M}. \tag{10}$$

Convergence is reached when the sums for $(M-1)$ and M do not differ by more than a given small number. It is important to calculate the summation for all atoms in the basis in the same way in order to avoid the appearance of demagnetization factors [28]. The sum converges, however, if the summation over the unit cell is taken first, due to the charge neutrality of the unit cell [28]. The summation is then taken over the polyhedron defined

by (10). There exist also methods to ensure faster convergence of the lattice sum, one by Artman and Murphy [20] and one by De Wette and Nijboer [28]. Such calculations gave the same results as the much simpler direct summation, which was usually preferred.

For the EFG at an Al site in Al_2O_3 the results of spherical summation and the summation over the polyhedron are compared in figures 1(*a*) and (*b*). For the spherical summation, the abscissa is the cut-off radius of the sphere around the probe atom in which all charges are taken into account, while for the polyhedron summation the number M, defined in equation (10), is given. In the case of Al_2O_3 with a lattice constant of $a = 5.128$ Å, $M = 10$ corresponds to a polyhedron with an edge length of 102.6 Å and is therefore comparable to a cut-off radius of 50 Å. For all calculations in this paper the summation was taken over the polyhedron. In figures 1(*c*)–(*f*) the different summation procedures are compared for Mn_2O_3, where the EFG is not axially symmetric. Figures 1(*e*) and (*f*) show that the asymmetry parameter η stabilizes for the same cut-off parameter as ν_Q. Convergence was assumed if the results of all six tensor components V_{ij} did not differ by more than 10^{-5} e Å^{-3}. For an axially symmetric tensor this corresponds to a change in the coupling constant of less than 2.8×10^{-4} MHz. The curves in figure 1 are plotted far beyond the convergence point.

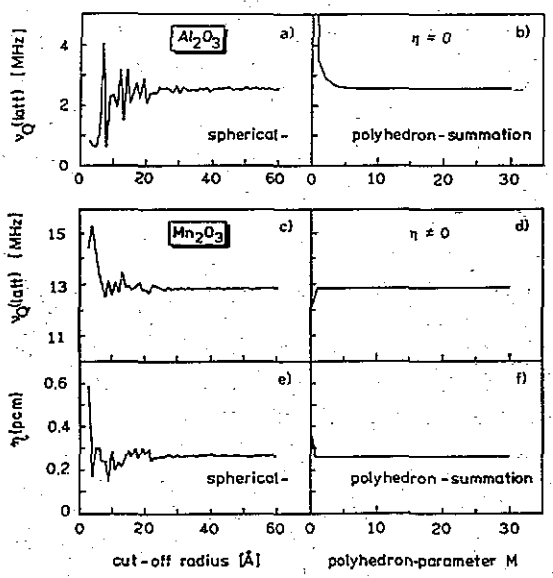

Figure 1. Convergence of the EFG in the point charge model for spherical (left) and polyhedron (right) summation: (*a*, *b*) ^{111}Cd in Al_2O_3 ($\eta = 0$); (*c*–*f*) ^{111}Cd in Mn_2O_3 ($\eta \neq 0$).

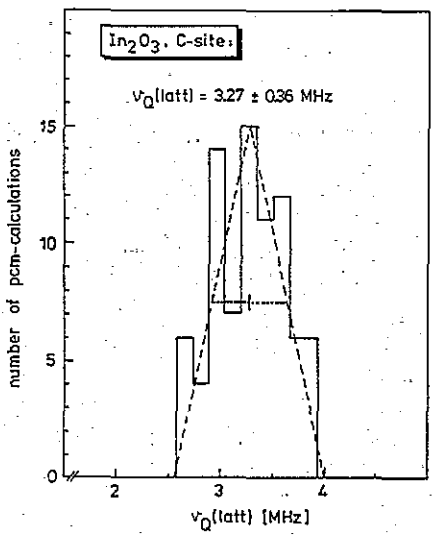

Figure 2. Distribution of ν_Q(latt) for various oxygen positions for the case of the C site in In_2O_3.

4.1. Shielding factors

If the distortion of the probe atom's electronic shell due to the external crystal field is not considered in a self-consistent field calculation, it has to be accounted for by suitable shielding factors [14–16]. Shielding factors γ_∞, which describe the enhancement of the EFG due to an infinitely far away charge, have been calculated for several atoms [16]. The

measured field gradient is then expressed as

$$V_{ij}^{\text{nucleus}} = (1 - \gamma_\infty) V_{ij}^{\text{ext}} \tag{11}$$

if V_{ij}^{ext} is the EFG produced by the external charges at the site of the probe nucleus. Relativistic Hartree–Fock–Slater calculations of γ_∞ were carried out by Feiock and Johnson [16]. Most ions with high atomic number Z show a negative sign of γ_∞ leading to an enhancement of the EFG V_{ij}^{ext}. The reported value for ^{111}Cd is $\gamma_\infty = -29.27$ [16].

If the electronic shell itself produces an additional term V_{ij}^{shell}, the total EFG can be written as [5, 6]

$$V_{ij}^{\text{nucleus}} = (1 - \gamma_\infty) V_{ij}^{\text{ext}} + (1 - R) V_{ij}^{\text{shell}}. \tag{12}$$

Beri *et al* [12] showed for α-Fe_2O_3 that further contributions to the EFG have to be considered and that every contribution has a distinctly different effective shielding factor. Once again, these calculations have not been performed for impurity atoms.

There exist theoretical predictions for the radial dependence of the shielding factors for different probe atoms [30]. Here the effect of a point charge at different distances from the electronic shell of the probe atom has been calculated without accounting for a charge transfer between shell and point charge. For distances below the mean radius of a 2s electron no screening is observed. Only for higher distances does the shielding factor increase and for large distances the total shielding factor of γ_∞ is reached [30]. Arends *et al* [30] suggested a parametrization of this behaviour:

$$\gamma(r) = \gamma_\infty [\![1 - \{1 + \exp[(r - r_0)/r_1]\}^{-1}]\!] \tag{13}$$

where r_0 and r_1 are adjustable parameters.

4.2. *PCM error estimations*

Especially in the case of the oxides crystallizing in the bixbyite structure, the different sets of coordinates have a large effect on the calculated hyperfine parameters. This fact was exploited by Bartos *et al* [32] who were able to refine the atomic positions by means of the measured HFI parameters assuming a fixed value of $\beta_\infty = (1 - \gamma_\infty) = 30.27$ for the shielding factor. Nevertheless, errors of the structure data are a common problem in performing PCM calculations in oxides, which has not been taken into account up to now. The possible errors of the HFI parameters were estimated by calculating the EFG for the values $p - \Delta p$, p and $p + \Delta p$ of every crystal parameter p. For each combination of all p, a PCM calculation was performed which gave a value for ν_Q(latt) and η(pcm). As the result either a triangular or a Gaussian distribution for ν_Q(latt) and for η(pcm) was obtained. As an example figure 2 shows the distribution of ν_Q(latt) for the C site of In_2O_3 for the coordinates obtained with Cu Kα radiation, reported in [33]. For the sake of simplicity, the mean values of these distributions and their widths σ were adopted in the following discussion and are listed in the tables. The coordinates used in the calculations are either the most recent x-ray data or, if available, single-crystal neutron diffraction data. It should be mentioned that the 'naive choice' of the coordinates, without considering any errors, in most cases was in reasonably good agreement with the mean values. If there are no high-accuracy determinations of the atomic positions, an uncertainty of the PCM of 5–12% has to be expected.

In figure 3, we plot the calculated EFG

$$\nu_Q(\text{pcm}) = (1 - \gamma_\infty)\nu_Q(\text{latt}) = 30.27\nu_Q(\text{latt}) \tag{14}$$

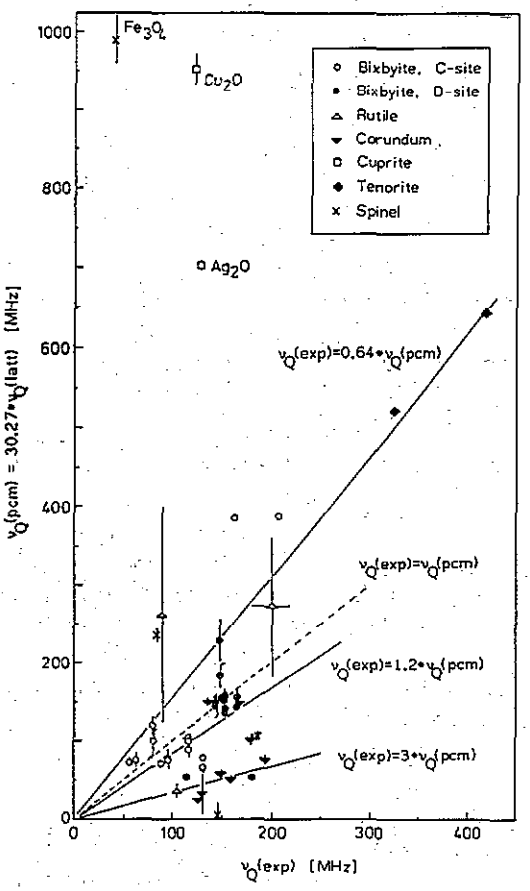

Figure 3. The predicted coupling constant $\nu_Q(\text{pcm}) = \beta_\infty \nu_Q(\text{latt})$ is plotted versus the experimental value $\nu_Q(\text{exp})$.

versus the experimentally determined $\nu_Q(\text{exp})$ to give a first impression of the consistency of the approach. The scatter is dominated by the error of the PCM results, whereas the experimental uncertainty of ν_Q is usually smaller than the dot size. Figure 3 will be discussed below.

A different way of presenting this comparison is plotting the ratio $\beta(\text{exp}) = \nu_Q(\text{exp})/\nu_Q(\text{pcm})$ (cf figure 4). This allows deviations from the 'standard' shielding factor to be tested. As we expect a radial dependence, $\beta(\text{exp})$ is plotted versus the average bond length $\langle d \rangle$ which averages over the distances between the probe and all next-neighbour oxygen atoms. Again, individual numbers can be found in the tables.

5. Discussion

Returning to figure 3 we see a clustering of data points along the dotted line $\nu_Q(\text{exp}) = 30.27\nu_Q(\text{latt}) = \nu_Q(\text{pcm})$. These are mainly the bixbyite data. A second line $\nu_Q(\text{exp}) = 3\nu_Q(\text{pcm})$ is clearly distinguishable which describes many corundum oxides. The two tenorite values (CuO and AgO) correspond to $\nu_Q(\text{exp}) = 0.64\nu_Q(\text{pcm})$. This line represents an upper limit for the bixbyite data cluster; the corresponding lower limit is given by

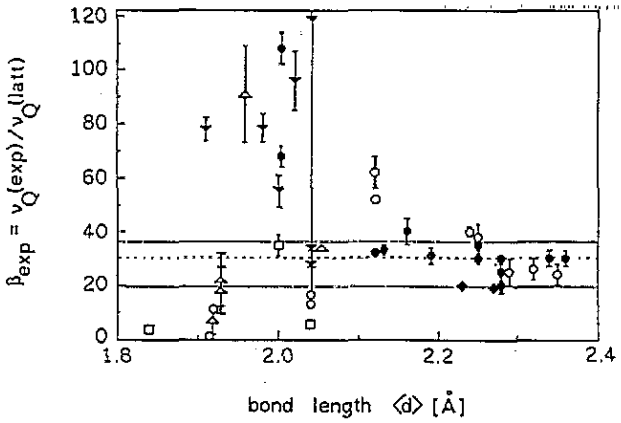

Figure 4. The experimental shielding factor $\beta(\text{exp}) = \nu_Q(\text{exp})/\nu_Q(\text{pcm})$ is plotted versus the average Cd–O bond length $\langle d \rangle$.

$\nu_Q(\text{exp}) = 1.2\nu_Q(\text{pcm})$. Completely outside these regions we find the two cuprites Ag_2O and Cu_2O and less far away from the line $\nu_Q(\text{exp}) = \nu_Q(\text{latt})$ the D-site data of β-Fe_2O_3 and Mn_2O_3.

One might ask what causes such a clear difference between the group of corundum oxides and the D site of the bixbyites: in both cases $^{111}In/^{111}Cd$ sits at the centre of a fairly regular oxygen octahedron. The mean bond length in the bixbyites is about $d \simeq 2.2$ Å, i.e. considerably larger than in the corundum class with $d \simeq 1.95$ Å. For that reason we have listed the average distance to the next neighbours, $\langle d \rangle$, in the table and have used $\langle d \rangle$ as abscissa in figure 4. For purely ionic bonding with bond lengths large enough to justify the use of γ_∞, equation (11) should be a good approximation. Indeed, for bond lengths larger than $d \simeq 2.1$ Å the weighted average value of the experimental shielding factors $\beta(\text{exp})$ is 32.3 ± 2.4, which is in perfect agreement with the theoretical value of $\beta_\infty = 30.27$ [16]. On the other hand, if we use the limits found in figure 3, we see in figure 4 nearly all data within the range $19 \leqslant \beta(\text{exp}) \leqslant 36$ for $\langle d \rangle \geqslant 2.1$ Å. The rather large experimental errors of the crystal parameters in the oxides partly account for the scatter of the $\beta(\text{exp})$ values.

For $\langle d \rangle \leqslant 2.05$ Å, the data seem to split into two groups, one centred around $\beta(\text{exp}) \simeq 85$ and the other one falling below $\beta(\text{exp}) = 10$. In earlier publications [1, 34] we attributed the high $\beta(\text{exp})$ value to the corundum structure, but now with this much larger data base, it becomes evident that bixbyites and rutile also show a large $\beta(\text{exp})$ if the bond length is small enough. The bond length $d = 2.1$ Å finds a convincing explanation if we calculate the sum of the radii of Cd^{2+} and O^{2-} ions. Using the radii listed by Pauling [35], we obtain $d_{cov} \simeq 2.1$ Å and $d_{ion} \simeq 2.5$ Å. These figures suggest that above $d \simeq 2.1$ Å the probe atom is predominantly in an ionic bond for which case equation (11) is a good approximation. For smaller bond lengths the electronic shell is altered due to a contribution of covalent bonding and therefore a new contribution to the EFG arises. Different signs of this contribution may explain the 'splitting' of the $\beta(\text{exp})$ values into two subgroups. The influence of covalent bonding was also shown by the MSX_α calculations of Nagel in Cu_2O [13] where the EFG of the O–Cd–O bond is predominantly due to the covalent contributions of the p orbitals.

A different consequence of covalent bonding could be that ^{111}Cd introduces lattice distortions which are obviously necessary if $^{111}In/^{111}Cd$ has to be placed within short bond

lengths. In the case of the rutile TiO_2, such distortions have been considered in the PCM by calculating the shifts in the nearest-neighbour shell and, indeed, a better agreement between experimental and theoretical HFI parameters was reached [36].

In the following we compare the experimental asymmetry parameters with those calculated by the PCM. In the PCM the axial symmetry of the EFG ($\eta = 0$) will be preserved even if the experimental errrors in the crystal parameters are taken into account. This is due to the fact that specific point symmetry groups are fixed. In such cases the average distance $\langle d \rangle$, given in the tables, reflects only the error of the lattice constants which is smaller by one order of magnitude. As a consequence, if the local environment is highly symmetric, one obtains an axially symmetric EFG, regardless of the shift parameters used for this point symmetry group. This is true for the oxides crystallizing in the corundum structure and for the symmetric D site in the bixbyite structure. In these cases the data yield $\eta \simeq 0$. For $\eta \neq 0$ the shift parameters used for the refinement of the specific point symmetry group can substantially alter η(exp) and therefore introduce rather large uncertainties in η.

In figure 5 we plot the ratio $\eta(\text{exp})/\eta(\text{pcm})$ versus the average bond length $\langle d \rangle$. The figure contains the data of rutile and the C-site bixbyite oxides. Again, above a bond length of $d \simeq 2.1$Å the agreement between experimental and theoretical data is rather good. Below this bond length η(pcm) clearly exceeds η(exp). Rather large deviations occur again in the cases of β-Fe_2O_3 and Mn_2O_3 where the experimental value of $\eta(\text{exp}) \simeq 0.6$ is at variance with the theoretical value $\eta(\text{pcm}) = 0.27$. A similar disagreement is visible in the case of Sc_2O_3 if we use the coordinates of [37], but not if we use the coordinates of [38]. This again demonstrates that the crystal parameters have a crucial effect on the PCM results.

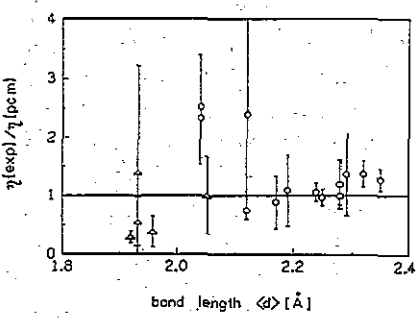

Figure 5. The ratio $\eta(\text{exp})/\eta(\text{pcm})$ is plotted versus the average Cd–O bond length $\langle d \rangle$.

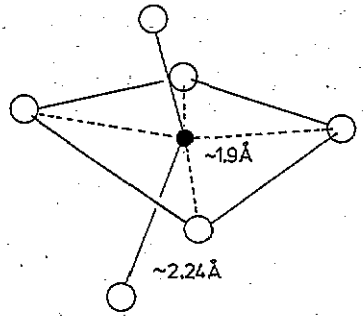

Figure 6. Structure of the irregular oxygen octahedron (D site) in the bixbyite Mn_2O_3.

As the two bixbyite oxides β-Fe_2O_3 and Mn_2O_3 are clearly deviate from the systematics of figures 4 and 5, we show the local structure of the irregular site in the Mn_2O_3 in figure 6. The bond lengths range between 1.89 and 2.24 Å and therefore cover a region where, according to figure 3, the experimental shielding factor will change dramatically. Therefore we tested in this case a radial-dependent shielding factor, using the parametrization given in equation (13), which still does not take into account any covalent bonding of the probe atom. Values for r_0 and r_1 were chosen yielding $\gamma(r) \simeq 0$ for $r \leqslant 1.5$, where according to Foley and Tycko [30] no screening occurs, and $\gamma(r) \simeq \gamma_\infty$ for $r \geqslant 2.1$ Å where a constant shielding factor $\gamma(r) = \gamma_\infty$ is sufficient to describe the data. The chosen values of $r_0 = 2.0$ and $r_1 = 0.1$ are not unambiguous, but reproduce the trend of the dependence of the coupling constant and the asymmetry parameter. This phenomenological approach results in $\nu_Q(\text{pcm}) = \gamma(r)\nu_Q(\text{latt}) = 165.5(9)$ MHz with $\eta = 0.66(3)$ for the C site. For the

symmetrical D site, $\nu_Q(\text{pcm}) = 60(2)$ MHz and $\eta = 0$ were calculated. Only in this case does the radially-dependent shielding factor give better agreement with the experimental HFI parameters. However, in the rutile oxides TiO_2 and SnO_2 the theoretical asymmetry parameters are still higher than the experimental values. This may point to lattice distortions due to the probe atom [36].

6. Conclusion

The systematics of EFGs at substitutional ^{111}Cd in binary oxides presented here combines, for the first time, the hyperfine parameters of always the *same* impurity atom in several classes of compounds with different crystal structures, ionicities, magnetic and conduction properties but the *same* atoms as the next neighbours. In many oxides the PCM has been shown to be a good approximation for calculating the EFGs. The calculated values crucially depend on the crystal parameters and their experimental errors. This can cause a problem in oxides as the oxygen coordinates are often not very precisely known. Within these PCM errors, a good agreement between experiment and calculation was found for bond lengths larger than $d \simeq 2.1$ Å. Here the theoretical shielding factor $\beta_\infty = 30.27$ for an infinitely far away charge can be used. This distance corresponds to the sum of the radii of an O^{2-} and a Cd^{2+} ion.

At smaller distances, where overlapping orbitals are present, the bonding and the electronic shell of the probe atom are changed and therefore other contributions to the EFG have to be considered. The data at shorter distances indicate that the extra EFG may have a different sign compared to that of V_{33}(latt). Furthermore, the calculated asymmetry parameters do not fit to the experimental ones. This one may take as a hint that the extra EFG has a different sign *and* orientation. Alternatively we assume that the probe causes a distortion among its next neighbours as suggested in TiO_2 and SnO_2 [36]. Such a distortion is more probable in the case of short bondlength. It would cause a different EFG, but the distortion cannot be predicted by the PCM. The use of a radially-dependent shielding factor, in a parametrization given by Arends and Pleiter [31], proved to be useful in some cases where the bond length varied over a large range for one specific local environment as for example in Mn_2O_3 in comparison with other bixbyite oxides.

Despite the success of the PCM in predicting the EFG at ^{111}Cd in oxides with the Cd–O bondlength exceeding 2.1 Å, a better theoretical understanding of the EFG would be desirable which could be achieved, e.g., by performing *ab initio* calculations. The large amount of new experimental data collected here might initiate a new attack upon this still unsolved problem.

Acknowledgments

The authors thank Th Wenzel for many fruitful discussions and A Pasquevich, D Lupascu and M Neubauer for the permission to quote some results prior to publication. The work was supported by the DFG.

References

[1] Bolse W, Uhrmacher M and Lieb K P 1987 *Phys. Rev.* **36** 1818

Bolse W, Bartos A, Kesten J, Lieb K P and Uhrmacher M 1989 *Ber. Bunsenges. Phys. Chem.* **93** 1285
[2] Hohenemser C, Kaqchnowski T and Bergstresser T K 1976 *Phys. Rev.* B **13** 3154
[3] Bartos A, Lieb K P, Pasquevich A F and Uhrmacher M 1991 *Phys. Lett.* **157A** 513
[4] Wiarda D, Wenzel T, Uhrmacher M and Lieb K P 1992 *J. Phys. Chem. Solids* **53** 1199
[5] Kaufmann E N and Vianden R J 1979 *Rev. Mod. Phys.* **51** 161
[6] Vandenberghe R E and De Grave E 1989 *Mössbauer Spectroscopy Applied to Inorganic Chemistry* vol 3, ed G J Long and F Grandjean (New York: Plenum)
[7] Nagel S 1985 *J. Phys. C: Solid State Phys.* **18** 3673
[8] Blaha P and Schwarz K 1989 *Hyperfine Interact.* **52** 153
[9] Schwarz K, Ambrosch-Draxl C and Blaha P 1990 *Phys. Rev.* B **42** 2051
[10] Kranefeld H and Fritsche L 1992 private communication
[11] Nagel S 1987 private communication
[12] Beri A C, Taesul Lee, Das T P and Sternheimer R M 1983 *Phys. Rev.* **28** 2335
[13] Nagel S 1985 *J. Phys. Chem. Solids* **46** 743
[14] Dalgarno A 1962 *Adv. Phys.* **11** 281
[15] Cohen M H and Reif F 1957 *Solid State Physics* vol 5 (New York: Academic) p 322
[16] Feiock F D and Johnson W R 1969 *Phys. Rev.* **187** 39
[17] Frauenfelder H and Steffen R M 1965 *Alpha-, Beta-, and Gamma-Ray-Spectroscopy* vol 2, ed K Siegbahn (Amsterdam: North-Holland) p 997
[18] Arends A R, Hohenemser C, Pleiter F, de Waard H, Chow L and Suter R M 1980 *Hyperfine Interact.* **8** 191
[19] Bersohn R 1958 *J. Chem. Phys.* **29** 326
[20] Artman J O and Murphy J C 1964 *Phys. Rev.* A **135** 1622
[21] Sharma R R and Das T P 1964 *J. Chem. Phys.* **41** 3581
[22] Taylor D R 1968 *J. Chem. Phys.* **48** 536
[23] Hafner S and Raymond M 1968 *J. Chem. Phys.* **49** 3570; 1970 *J. Chem. Phys.* **52** 279
[24] Sawatzky G A and Hupkes J 1970 *Phys. Rev. Lett.* **25** 100
[25] Sharma R R 1970 *Phys. Rev. Lett.* **25** 1622
[26] Wykoff R W G 1963 *Crystal Structures* (New York: Interscience)
[27] Bolse W, Uhrmacher M and Kesten J 1987 *Hyperfine Interact.* **35** 931
[28] Nijboer B R A and De Wette F W 1957 *Physica* **23** 309
De Wette F W 1961 *Phys. Rev.* **123** 103
De Wette F W and Schacher G E 1965 *Phys. Rev.* A **137** 92
Nijboer B R and De Wette F W 1958 *Physica* **24** 422
[29] Ashcroft N W and Mermin N D 1981 *Solid State Physics* (Tokyo: Holt-Saunders Int. Edition)
[30] Foley H M and Tycko R 1954 *Phys. Rev.* **93** 734
[31] Arends A R and Pleiter F 1982 *Hyperfine Interact.* **12** 143
[32] Bartos A, Lieb K P, Uhrmacher M and Wiarda D 1993 *Acta Crystallogr.* B **49** 165
[33] Marezio M 1966 *Acta Crystallogr.* **20** 723
[34] Kesten J, Bolse W and Lieb K P 1990 *Hyperfine Interact.* **60** 683
[35] Pauling L 1948 *The Nature of the Chemical Bond* (Oxford: Oxford University Press)
[36] Wenzel T, Bartos A, Lieb K P, Uhrmacher M and Wiarda D 1992 *Ann. Phys., Lpz.* **1** 155
[37] Geller S, Romo P and Remeika J P 1967 *Z. Kristallogr.* **124** 136
[38] Norrestan R 1968 *Ark. Kemi* **29** 343
[39] Smrcok L 1989 *Cryst. Res. Technol.* **24** 607
O'Connor B H and Valentine T U 1969 *Acta Crystallogr.* B **25** 2140
Paton M G and Maslur E N 1965 *Acta Crystallogr.* **19** 307
Scott H G 1981 *Acta Crystallogr.* A **37** 956
[40] Hase W 1963 *Phys. Status Solidi* **3** K446
[41] Fert A 1962 *Bull. Soc. Fr. Minéral. Cristallogr.* **85** 267
[42] Moon R M, Koehler W C, Child H R and Raubenheimer L J 1968 *Phys. Rev.* **176** 722
[43] Shitu J, Wiarda D, Wenzel T, Uhrmacher M, Lieb K P, Bedi S and Bartos A 1992 *Phys. Rev.* B **46** 7987
[44] Gashuro G and Soves O J 1970 *Acta Crystallogr.* B **26** 938
[45] Geller S 1971 *Acta Crystallogr.* B **27** 821
[46] Ikeda Y, Takano M and Bando Y 1987 *Bull. Inst. Chem. Res. Kyoto Univ.* **64** 249
[47] Wenzel T 1990 *Diplomarbeit* Universität Göttingen, unpublished
[48] Renteria M, Bibiloni A G , Moreno M S, Desimoni J, Mercader R C, Bartos A, Uhrmacher M and Lieb K P 1991 *J. Phys.: Condens. Matter* **3** 3628
[49] Gervais F and Kress W 1985 *Phys. Rev.* B **31** 4809

[50] Naicker V, Bartos A, Lieb K P, Uhrmacher M, Wenzel T and Wiarda D 1993 *IX HFI-Conf. (Osaka) Hyperfine Interact.* at press
[51] Marinder B O 1961 *Acta Chem. Scand.* **15** 707
Pynn R, Axe J D and Thomas R 1976 *Phys. Rev.* B **13** 2965
[52] Teraro N 1963 *Japan. J. Appl. Phys.* **2** 156
[53] Renteria M, Wiarda D, Biblioni A G and Lieb K P 1990 *Hyperfine Interact.* **60** 679
[54] Wiarda D 1992 *Doctoral Thesis* Göttingen, unpublished
[55] Kesten J 1989 *Hyperfine Interact.* **52** 17
[56] Kesten J, Uhrmacher M and Lieb K P 1990 *Hyperfine Interact.* **59** 309
[57] Neubauer M 1993 private communication
[58] Coey J M D 1970 *Acta Crystallogr.* B **26** 1876
[59] Forker M, Saitovich H and des Jesus Silva P P 1984 *J. Phys. C: Solid State Phys.* **17** 1055
[60] Asai K, Ambe F, Okadda T and Sekizawa H 1990 *Phys. Rev.* B **41** 6124
[61] Marezio M and Remeika J P 1967 *J. Chem. Phys.* **46** 1862
[62] Pasquevich A F, Uhrmacher M, Ziegeler L and Lieb K P 1993 *Phys. Rev.* B submitted
[63] Bartos A, Bolse W, Lieb K P and Uhrmacher M 1988 *Phys. Lett.* **130A** 177
[64] Roth W L 1964 *J. Phys. Chem. Solids* **25** 1
[65] Inglot Z and Wegner D 1991 *J. Phys.: Condens. Matter* **3** 2137
[66] Buhl A 1969 *J. Phys. Chem. Solids* **30** 805
[67] Hamilton W C 1958 *Phys. Rev.* **110** 1050
Cross B J and Westruns E F 1972 *Phys. Rev.* B **5** 3791
[68] Forsyth J B, Brown J D and Wanklyn B M 1988 *J. Phys. C: Solid State Phys.* **21** 2917
Asbrink S and Norrby L J 1970 *Acta Crystallogr.* B **26** 8
[69] Wegner D, Inglot Z and Lieb K P 1990 *Ber. Bunsenges. Phys. Chem.* **94** 1
[70] Inglot Z, Wiarda D, Lieb K P, Wenzel T and Uhrmacher M 1991 *J. Phys.: Condens. Matter* **3** 4569